Chemical Engineering Science 211 (2020) 115308

Contents lists available at ScienceDirect

Chemical Engineering Science

journal homepage: www.elsevier.com/locate/ces

Extending estimation of the critical deposition velocity in solid–liquid pipe flow to ideal and non-ideal particles at low and intermediate solid volume fractions

Hugh P. Rice [a,1,*], Jeffrey Peakall [b], Michael Fairweather [a], Timothy N. Hunter [a]

[a] School of Chemical and Process Engineering, University of Leeds, Leeds LS2 9JT, United Kingdom
[b] School of Earth and Environment, University of Leeds, Leeds LS2 9JT, United Kingdom

HIGHLIGHTS

- Critical deposition velocity separates suspended and bed-forming particle-laden flows.
- Data from new experiments using acoustic method combined with data from literature.
- Relationship found between critical deposition velocity and material/flow properties.
- Volume factor accounts for non-ideal behaviour of solid particles such as aggregation.
- Correlation found between volume factor and packing fraction of solid phase.

ARTICLE INFO

Article history:
Received 24 May 2019
Received in revised form 3 October 2019
Accepted 18 October 2019
Available online 21 October 2019

Keywords:
Particle-laden flow
Acoustic measurements
Ultrasonics
Sediment transport
Radioactive waste

ABSTRACT

The critical deposition velocity in horizontal pipe flow of liquid-solid slurries separates bed-forming and fully suspended flows. A compilation of critical deposition velocity data is presented using new experimental data (for particles ranging from 9 to 690 μm in diameter) along with data from the literature, and a close correlation between the particle Reynolds number and the Archimedes number (which describe the properties of the flow and the liquid and solid phases) is found. The role of solid particle packing is discussed and suggestions are made for the incorporation of solid-phase material properties – specifically particle shape and angularity, and surface forces – into an empirical parameter, the volume factor, α, to account for the deviation of particle behaviour from ideal, non-interacting, hard-sphere behaviour.

1. Introduction

Solid-liquid slurry flows can be categorized into fully suspended and homogeneous (or pseudo-homogeneous); heterogeneous, in which a solids concentration gradient exists; flow with moving bed (or saltation flow or "two-layer" flow); flow with a stationary bed (sometimes "three-layer" flow) (Peysson et al., 2009; Rice et al., 2017); and plug flow, in which the solid span the conduit and move *en masse* (Crowe, 2006; Doron and Barnea, 1995; Wasp et al., 1977). Each of these flow regimes, which are illustrated in idealised form elsewhere (Doron and Barnea, 1996; Gillies and Shook, 1991; Rice et al., 2015), can be distinguished by a critical velocity or flow rate, which are essential flow parameters for operators working with high-value or hazardous substances in the food, nuclear and minerals processing industries, for example (Bux et al., 2017; Poloski et al., 2010; Thomas, 1961,1962) because of the associated pumping and energy requirements, the possibility of blockages and, in the case of stationary deposits of chemically or radiologically active materials, the increased risk of corrosion, heat deposition and elevated radiation dose to operators.

These critical velocities, such as the critical deposition velocity (CDV), which delineates bed-forming and fully suspended flows of liquid–solid mixtures, slurries and sludges, have received extensive theoretical and practical attention. They are defined in a variety of ways, such as the pick-up velocity, saltation velocity, critical velocity and suspending velocity (Bain and Bonnington, 1970; Crowe, 2006; Peker and Helvacı, 2007; Rabinovich and Kalman, 2011; Spells, 1955) and some ambiguity over the relationship between the various definitions persists.

* Corresponding author.
E-mail address: h.p.rice@leeds.ac.uk (H.P. Rice).
[1] Current address: School of Mechanical Engineering, University of Leeds, Leeds LS2 9JT, United Kingdom.

https://doi.org/10.1016/j.ces.2019.115308
0009-2509/

A similarly large range of experimental and numerical methods, theoretical models and empirical correlations exist for measuring and predicting such transitional velocities (Gillies et al., 1991; Oroskar and Turian, 1980; Soepyan et al., 2014; Turian et al., 1987), *e.g.*, minimum pressure drop with respect to flow rate (Goedde, 1978), acoustic bed depth measurement (Rice et al., 2015), visual assessment of deposition (Thomas, 1961), and the onset of motion of individual particles (Clark et al., 2015). However, the predictions of such models often disagree with each other and with experimental results (Al-lababidi et al., 2012; Miedema, 2016), and this lack of clarity gives operators less predictive certainty in terms of flow assurance and safety: using too low a pump rate encourages solids deposition and increases the risk of plugging, whereas too high a flow rate increases energy costs and the risk of wear in conduits and pumping equipment.

The UK and USA have large and complex nuclear legacy waste inventories that are physically, chemically and radiologically diverse. In the UK, the majority is stored at the Sellafield site, whereas in the USA the waste is more widely distributed; however, the Hanford Site, Washington, is the most contaminated. On both sites, an ongoing challenge exists to transport, store, process and dispose of the waste inventories safely and economically. A number of reviews of models and correlations for predicting critical deposition velocities – as they pertain to nuclear waste slurries at the Hanford Site specifically – are available. Welch (2001) reviewed the most significant engineering and scientific obstacles present at Hanford and investigated the suitability of the Oroskar and Turian (1980) CDV correlation. Liddell and Burnett (2000) reviewed several correlations and recommended those of Gillies and Shook (1991) and Oroskar and Turian (1980) for slurry flow prediction at Hanford. More recently, Poloski et al. (2010) described the difficulty in representing slurries with complex compositions and presented a correlation for the CDV with two regimes separated by particle material properties. However, it is noted that both the Gillies and Shook (1991) and Oroskar and Turian (1980) correlations do not capture the correct behaviour at low solids loadings: both predict a CDV of zero in this limit, whereas in reality a non-zero value is obtained, *i.e.*, for individual solid particles (Rice et al., 2015), referred to variously as the equilibrium velocity, pick-up velocity and saltation velocity, depending on the exact mechanism, by Soepyan et al. (2014), for example.

Rice et al. (2015) presented an unambiguous acoustic bed-depth measurement method for determining the CDV in horizontal, solid-liquid, cylindrical-pipe flow, and synthesised new experimental data with others from the literature, using strict data selection criteria described later, to establish a correlation between flow parameters, material properties and the CDV. It was shown that the correlation extended beyond the very dilute limit (Soepyan et al., 2014) and that no existing mathematical form of the CDV could account for the experimental data in the literature. Key questions remain as to the universality of CDV correlations for different systems, which is the focus of the present study. In particular, the CDV is measured for a wide range of particle sizes and densities, with three different species (glass, plastic and dense barium sulphate) that cover a large range of particle sizes and densities, using a high-resolution acoustic backscatter technique to characterise the consolidated sediment beds in a horizontal pipe loop. Importantly, the concentration ranges over which the CDV is measured is significantly increased over previous studies to clarify the range of validity of the empirical relationship previously determined by the current authors (Rice et al., 2015). In the following section (Sec. 2), the relationship between the CDV and material and flow parameters is reviewed and the objectives of the study are described, in terms of the range of solids loadings investigated, the data selection criteria employed and the effect of particle properties not accounted for through the mean particle diameter.

2. Theoretical background

In a review of a large number of data in the dilute limit (specifically $0 < \phi < 10^{-4}$, where ϕ is the solids volume fraction), Soepyan et al. (2014) found that a large number of models, when optimized, could be reduced to the following simple form:

$$\mathrm{Re}_{pc0} = 7.90\mathrm{Ar}^{0.41}, \tag{1}$$

where Re_{pc} is the particle Reynolds number, with the subscript "0" indicating the low-ϕ limit, and Ar is the Archimedes number. The particle Reynolds can be given by:

$$\mathrm{Re}_{pc} = \frac{U_c d}{\nu}, \tag{2}$$

where U_c is the CDV, d is the particle diameter and ν is the kinematic viscosity of the fluid. The Archimedes number, Ar, is given by:

$$\mathrm{Ar} = \frac{g d^3 (s-1)}{\nu^2}, \tag{3}$$

where g is the acceleration due to gravity, s is the ratio of solid to liquid densities, *i.e.*, $s = \rho_s/\rho_l$. Rice et al. (2015) presented results from an experimental study and a compilation of data from the literature – selected according to strict criteria, which are discussed and revised later – and derived a relationship between Re_{pc} and Ar that extended beyond the dilute limit, of the following form:

$$\mathrm{Re}_{pc} = a\mathrm{Ar}^b\left(1 + \alpha\phi^{0.5}\right) \tag{4}$$

where α is referred to hereafter as the volume factor. In the dilute limit, the value of Re_{pc} corresponding to pick-up, Re_{pc0}, is obtained such that $\mathrm{Re}_{pc0} = a\mathrm{Ar}^b$ in general. Rice et al. (2015) found the following correlation best fitted the available datasets up to volume fractions of several per cent:

$$\mathrm{Re}_{pc} = 12.4\mathrm{Ar}^{0.493}\left(1 + 8.91\phi^{0.5}\right) \tag{5}$$

The aims of this study are: (a) to investigate whether the validity of the $\phi^{0.5}$ term in Eq. (4) extends beyond volume fractions of a few per cent; (b) to present new experimental data at higher volume fractions; and (c) to supplement with additional datasets the 11 identified by Rice et al. (2015). The strict data selection criteria used by Rice et al. (2015) are also reviewed and relaxed. Lastly, the relationship between an empirical parameter that incorporates the deviation of solid materials' behaviour from ideal-sphere, the volume factor, α, and the maximum packing fraction of ideal and non-ideal particulate species is discussed in terms its influence on the CDV correlation.

3. Experimental methodology and data selction

3.1. Materials characterisation

Five solid particle species were used in the experiments: two glass species, two plastic species and barium sulphate, commonly known as barytes (sources: all Guyson International, Ltd., UK, except for barytes: RBH Ltd., UK). The glass particles are spherical in shape, while the plastic and barytes have a roughened morphology with non-spherical aspect ratios (see micrograph images of barytes in Bux et al., 2017; glass and plastic in supplementary material and Rice, 2013). The glass and plastic are low-cost, engineered blast media, while the barytes is a milled mineral and a common simulant for fine nuclear fission wastes (Bux et al., 2017). Particle size distributions were measured with Malvern Instruments *Mastersizer 2000E* and *Mastersizer 3000* laser diffraction sizers and the densities with a Micromeritics *AccuPyc 1300* pycnometer. In addition, the Corey shape factor, F_s (Corey, 1949; Dietrich, 1982) and Powers roundness factor, P (Powers, 1953;

Syvitski, 2007) have been measured previously for the large plastic species (Rice et al., 2017) with a Retsch *Camsizer XT* optical sizing instrument and were found to be $F_s = 0.842$ (where 0 corresponds to a rod and 1 to a sphere) and $P = 2.49$ (*i.e.*, sub-angular, where 0 corresponds to very angular and 6 to well rounded). Particle size distributions for the five species used in this study are shown in Fig. 1(a), along with log-normal fits to the measured data in Fig. 1(b); it is also noted that triangles, squares and circles are the symbols used to denote barytes, glass and plastic particles, respectively, in figures throughout this paper.

The packing fraction, ϕ_m, of the particle species were determined in two ways. The first, used for the glass and plastic species, was with dry particles in volumetric flasks of at least three sizes (50, 100, 250 and 500 ml) for each species, and no trend with flask size was found, confirming wall effects were not significant, as described by Rice et al. (2015). The second method, used for barytes, was to measure the settled bed depth in wet samples taken from the mixing tank of the pipe flow loop (see Section 3), and no variation in packing fraction was found with changes to nominal volume fraction or sample mass. For non-interacting species like glass and plastic, the first and second method should yield the same result; for surface-charged species like barytes, the result from each method may differ due to the effects of the fluid phase on interparticle interactions and so the second method was used for barytes, as it better represents the conditions in the flow experiments.

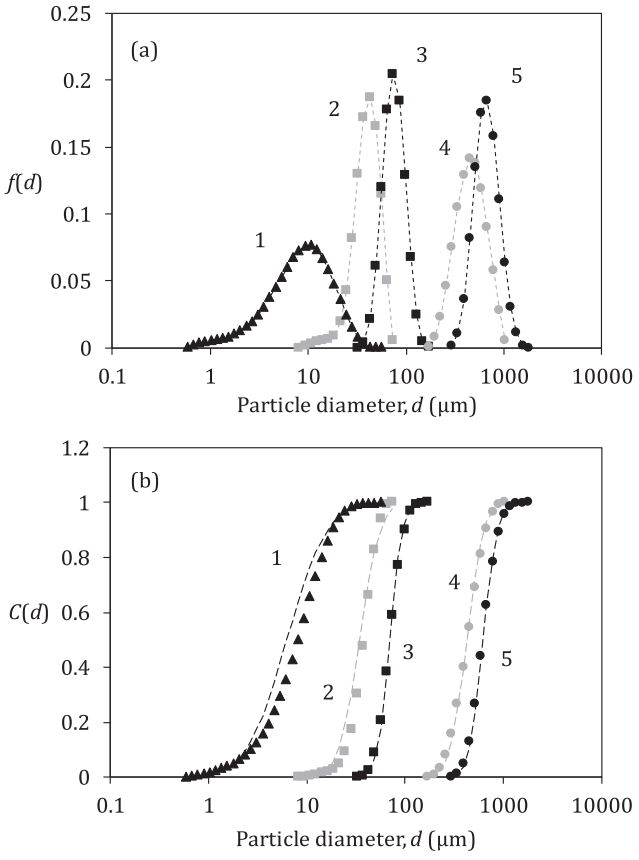

Fig. 1. (a) Particle size distributions by volume of species used in this study, measured with the *Mastersizer* instrument; dashed lines for legibility. (b) Cumulative distribution function (CDF) of particle size, with log-normal fits shown as dashed lines. (1) Barytes, (2) small glass, (3) large glass, (4) small plastic and (5) large plastic.

4. Literature data selection and analysis

A total of 14 datasets were compiled: five from the present experimental study and nine from the literature, for which strict selection criteria were applied (see below). For the current study, additional data for the glass and plastic systems from a previous study by Rice et al. (2015) at low volume fractions ($\phi < 2\%$) are included in the analysis that follows. As discussed, barytes was chosen for its utility as a nuclear waste simulant (Hunter et al., 2013; Paul et al., 2013) and is an ultrafine, micron-sized material with a surface charge (see Bux et al., 2017), a property that strongly influences sedimentation and resuspension behaviour.

Data from the literature were selected according to strict criteria, which were relaxed somewhat compared to those used by Rice et al. (2015). First, at least three data points at several volume fractions had to be available to ensure a reliable fit and enable accurate extrapolation to $\phi \to 0$. Second, the data had to be selected over a range of ϕ such that U_c shows a $\phi^{0.5}$ dependence. Third, at least two particle size data had to be available, so that the distribution is known or can be inferred (*e.g.*, modelled as log-normal). Fourth, the data must be specifically for critical deposition velocity, defined as that at which the solid phase is fully suspended, rather than any other critical velocity. These criteria were formulated in order that all flow and material properties are accounted for.

The literature on experimental determination of critical velocities is large – comprising thousands of data (Oroskar and Turian, 1980; Soepyan et al., 2014; Turian et al., 1987) – and mature, with few recent studies, but the majority of datasets did not satisfy the selection criteria given above and the scarcity of high-quality data is one motivation for this study. Of the datasets assessed (and some of the studies cited had both suitable and unsuitable datasets within them), many were rejected based principally on: the first or second criteria, which are similar (Goedde, 1978; Sinclair, 1962; Wasp et al., 1977; Worster and Denny, 1955); the third (Hayden et al., 1971; Parzonka et al., 1981; Spells, 1955); or the fourth, or were in a format that meant they were difficult to interpret or could not be converted into SI units (Babcock, 1970; Cairns et al., 1960; Durand and Condolios, 1952; Hughmark, 1961; Murphy et al., 1954; Newitt, 1955; Smith, 1955; Thomas, 1979; Thomas, 1961, 1962; Wilson, 1965).

All measured and derived properties of the solids species used in this study are given in Table 1 and Table 2 and Tables S1 and S2 in the supplementary material, where the datasets from the literature are also summarized (Al-lababidi et al., 2012; Graf et al., 1970; Parzonka et al., 1981; Sinclair, 1962), including several that are additional to those used by Rice et al. (2015). Particle size distributions for the five species used in this study are shown in Fig. 1.

5. Pipe flow loop and bed depth measurement method

The bed depth measurement method, which includes a correction for ambient suspended solids, is as described in detail by Rice et al. (2015) but is summarized here. First, a solid-liquid suspension with a known volume fraction of solids was circulated in a pipe flow loop (internal diameter $D = 42.6$ mm) at a high flow rate to minimise deposition throughout the apparatus, then reduced to a low flow rate for several minutes in order that a flat, stationary bed of settled solid particles is established along a transparent, horizontal test section. The flow rate was then increased incrementally and the bed depth allowed to equilibrate over several minutes at each flow rate. The pump was then turned off and the solids allowed to settle for seconds or minutes, depending on the material. The bed depth could then be measured using an acoustic backscatter system (as a more accurate, distinct bed depth measurement is possible with a settled bed than with a moving

Table 1
Physical and derived properties of particle species used in this study. D = 42.6 mm in all cases.

Substance	Particle size data (μm)			s[a]	Ar
	d_{10}	d_{50}	d_{90}		
Small glass, "Honite 22"	26.8	40.5[b]	56.6	2.45	0.945[b]
Large glass, "Honite 16"	53.5	74.8[b]	104	2.46	6.00[b]
Small plastic. "Guyblast 40/60"	269	451[b]	712	1.54	482[b]
Large plastic, "Guyblast 30/40"	459	659[b]	966	1.52	1450[b]
Barium sulphate	2.91	8.86	20.6	4.43	0.0234

[a] $s = \rho_s/\rho_l$, where ρ_s and ρ_l are densities of the solid and liquid phases, respectively.
[b] Updated using data at higher ϕ or corrected following review of Rice et al. (2015).

Table 2
Log-normal, packing fraction and derived properties of species used in present study. M and S are log-normal parameters.

Substance	M[a]	S[a]	ϕ_m	ϕ_{Farr}	Re_{pc0}	α
Small glass	3.54	0.386	0.619	0.686	9.01[b]	13.8[b]
Large glass	4.25	0.232	0.616	0.661	28.5[b]	7.79[b]
Small plastic	6.05	0.319	0.514	0.674	248[b]	4.13[b]
Large plastic	6.44	0.263	0.513	0.666	377[b]	4.68[b]
Barium sulphate	1.84	0.748	0.432	0.756	5.40	3.26

[a] M and S calculated using particle size data (in μm units) *via* linearization of Eq. (11).
[b] Updated using data at higher ϕ or corrected following review of Rice et al. (2015).

one), and the flow rate was increased until no settled bed was visible.

A geometric correction, δh, to the bed depth for ambient solids was applied; this correction accounts for solids that would remain suspended during flow, were the pump to be running, and is as follows:

$$\phi_m c \delta h = \phi A_{\text{flow}} \tag{6}$$

where ϕ_m is the maximum packing fraction of the solid species, c is the chord length of the bed surface (determined geometrically from the measured bed depth), ϕ is the (known) volume fraction of solids overall and A_{flow} is the flow cross-sectional (*i.e.*, that above the bed, also determined geometrically from the bed depth).

An off-the-shelf ultrasonic system was used to measure bed depth, consisting of a *UVP-DUO* signal processor (Met-Flow, Switzerland) and a monostatic (*i.e.*, emitter-receiver) transducer operating at 4 MHz (Imasonic, France), giving a spatial resolution of 0.37 mm. The transducer was mounted, perpendicular to the mean flow direction, on the test section. A variable centrifugal pump was used to control the flow rate, an impeller mixer to maintain a suspension in the mixing tank (nominal capacity 100 L, *i.e.*, 0.1 m^3) and an ultrasonic flow meter (Omega Engineering, UK) to measure the flow rate, Q, from which the mean axial flow velocity, U, is calculated such that $Q = \pi U D^2/4$.

6. Results and discussion

Bed depth results for three of the particle species (large glass, large plastic and barytes) are given at three volume fractions in Figs. 2, 3 and 4, respectively, where the x-intercept of a linear fit to the corrected bed-depth data gives the CDV, U_c, which is observed to increase with ϕ, for all solid species. CDV data for all particle species are listed in Table S1 in the supplementary material. It is noted that the volume fraction range accessible to measurement with barytes was lower than for either the glass or plastic particles. Indeed, at concentrations above ϕ = 2%, determination of the CDV from bed depth measurements became difficult as settling times became prohibitively long as a result of hindered settling (Richardson and Zaki, 1954; Vesilind, 1968). Very low, concentration-dependent settling velocities have been observed in suspensions of several nuclear-analogues (Paul et al., 2017) and magnesium hydroxide (Johnson et al., 2016).

Fig. 5 shows the variation of the CDV, U_c, with solids volume fraction for some examples of particle species: large glass, large plastic and barytes (present study) in Fig. 5(a) and two datasets from the literature (Parzonka et al., 1981; Sinclair, 1962) in Fig. 5(b). The square-root dependence of CDV on solids concentration was suggested by Thomas (1962) and Rice et al. (2015) and remains tentative. However, it is clear from Fig. 5 that U_c varies with $\phi^{0.5}$ over at least the range $0 < \phi^{0.5} < 0.4$ ($0 < \phi < 0.16$) or so for most particle species, *i.e.*, far beyond the dilute limit. However, caution must be taken regarding the upper concentration limit for fine particles with significant surface forces, such as the barytes, as discussed earlier. Nevertheless, for most systems studied (including the datasets taken from the literature) the square-root correlation appears valid up to a significant part of the solids volume fraction corresponding to the maximum CDV (as illustrated by Parzonka et al., 1981), which allows for the data selection criterion relating to volume fraction given by Rice et al. (2015) to be relaxed.

As described by Rice et al. (2015), the pick-up velocity, Re_{pc0}, can be found from the y-intercept of the plot of U_c *vs.* $\phi^{0.5}$, as in Fig. 5. Additionally, the volume factor, α (see the functional relationship of Re_{pc} in Eq. (4)) is found from the ratio of the gradient and y-intercept in the limit of $\phi \to 0$. The relationship between Re_{pc0} and Ar is then determined by fitting, in order to determine the parameters a and b (such that $\text{Re}_{pc0} = a\text{Ar}^b$), and a mean value of α for all particle species is taken to yield the following result for the five species used in this study, given in Fig. 6, where Re_{pc0} *vs.* Ar is plotted for all datasets; Re_{pc0} and α for all particle species used here are given in Table 2.

The final, explicit relationship for Re_{pc} (and thus U_c) with exponents and coefficients derived from Fig. 5 and Fig. 6 is given in Eq. (7) for the five species investigated in this study, while the corresponding relationship for all 14 datasets (*i.e.*, those from both this study and the literature) is given in Eq. (8).

$$\text{Re}_{pc} = 16.3\text{Ar}^{0.414}\left(1 + 6.73\phi^{0.5}\right) \tag{7}$$

$$\text{Re}_{pc} = 15.3\text{Ar}^{0.457}\left(1 + 9.04\phi^{0.5}\right) \tag{8}$$

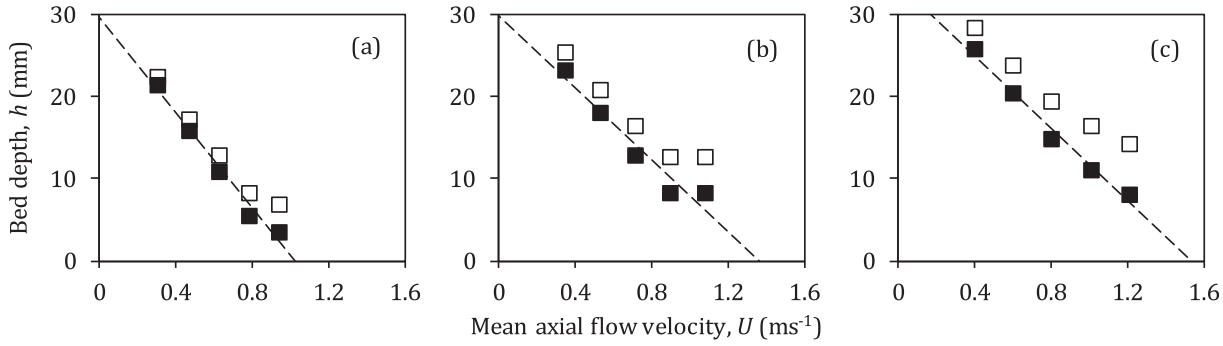

Fig. 2. Measured bed depth, h, *vs.* mean axial flow velocity, U, for large glass particles at (a) $\phi = 5\%$, (b) $\phi = 10\%$ and (c) $\phi = 15\%$. Open symbols: uncorrected data; filled symbols: corrected data. Correction procedure given by Rice et al. (2015) and summarised in text. Dashed line: linear fit to corrected data; intercept with x-axis gives critical deposition velocity, U_c.

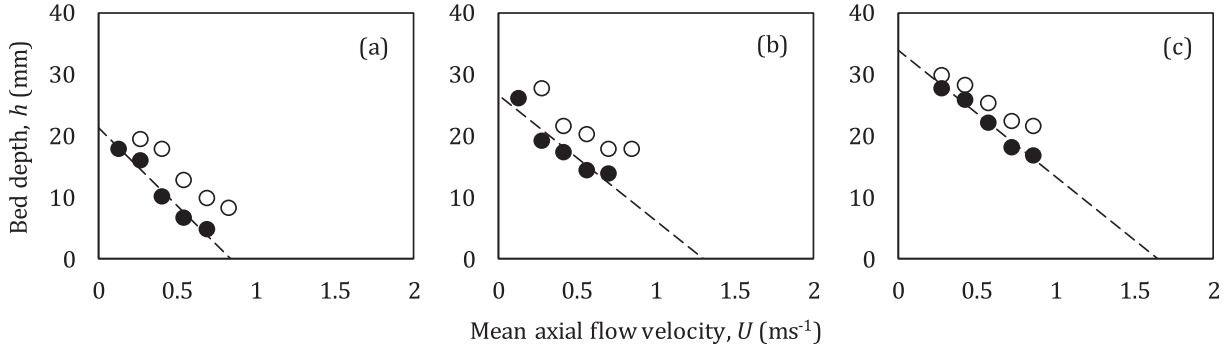

Fig. 3. Measured bed depth, h, *vs.* mean axial flow velocity, U, for large plastic particles at (a) $\phi = 5\%$, (b) $\phi = 10\%$ and (c) $\phi = 15\%$. Symbols, *etc.*, as Fig. 2.

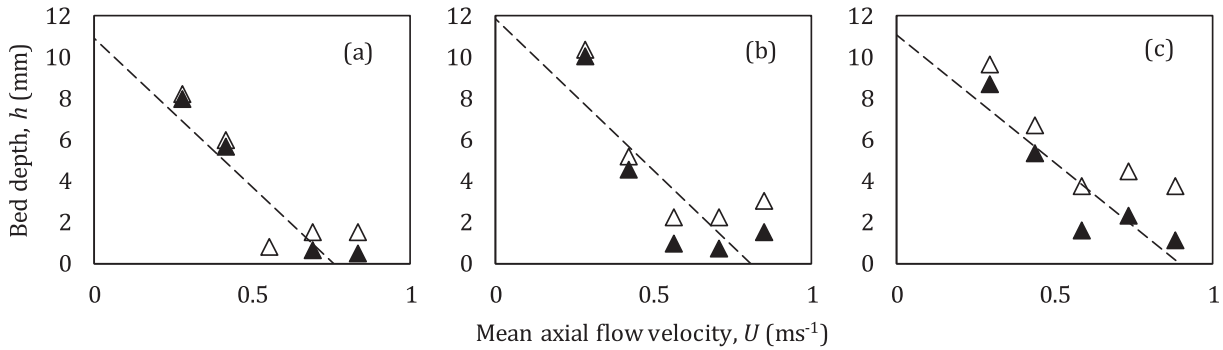

Fig. 4. Measured bed depth, h, *vs.* mean axial flow velocity, U, for barytes at (a) $\phi = 0.5\%$, (b) $\phi = 1\%$ and (c) $\phi = 2\%$. Symbols, *etc.*, as Fig. 2.

It is noted that the agreement between the limiting cases of Eqs. (7) and (8) (*i.e.*, for $\phi \to 0$) with the pick-up velocity relationship given by Soepyan et al. (2014) in terms of the exponent b (0.414, present data; 0.457, all data) is very good (0.41 in Soepyan et al., 2014), but the present results ($a = 16.2$, present data; 15.3, all data) suggest the Soepyan et al. (2014) relationship ($a = 7.90$) underestimates Re_{pc0} in general. It is important to note the subtle but important differences between the definitions of pick-up and incipient motion velocities used by Soepyan et al. (2014); however, in the case of zero bed depth, the mechanisms of pick-up and incipient motion are identical.

Measured values of Re_{pc} and those predicted by Eqs. (7) (present data) and (8) (all data) are shown in frames (a) and (b) of Fig. 7, respectively. Bounds corresponding to ± 30% are indicated in frame (a) and ± 100% in frame (b), demonstrating very good agreement between experiment and prediction. The degree of scatter in the data compares very favourably to that shown in other studies and reviews (Oroskar and Turian, 1980; Poloski et al., 2010; Turian et al., 1987).

As was the case in the study of Rice et al. (2015), the volume factor α, as defined in Eq. (4) and evaluated in Eq. (8), was calculated as a simple mean of the values for all particle species. This method serves not to give bias to any dataset with more points, but may not be ideal because the values of α (see Table 2 for particle species used in the present study and Table S2 in the supplementary material for those from the literature) span more than an order of magnitude, and the material properties that are presumably responsible for the variation in α – most likely shape, roughness, tendency to aggregate and surface forces, as discussed later – are not accounted for. To address this issue, a correlation was sought between the derived values of α and the measured values of the packing fraction, ϕ_m, for the five species used here only (see Table 2; packing fraction information was not available for the datasets taken from the literature). Broadly, as is clear from

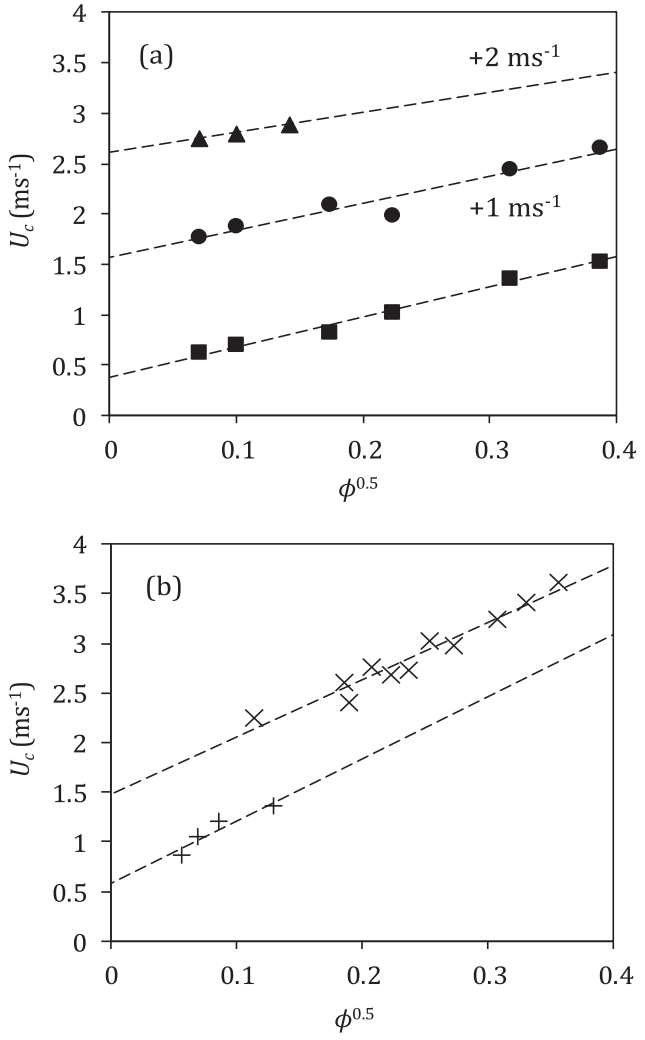

Fig. 5. Critical deposition velocity, U_c, *vs.* $\phi^{0.5}$, where ϕ is solids volume fraction. (a) Squares: large glass, circles: large plastic, triangles: barytes; all present study, offsets for better visualisation indicated in figure. (b) Crosses: unknown material (d_{50} = 90 μm, s = 3.00), series 7, Fig. 4 of Parzonka et al. (1981); pluses: iron in kerosene, from Sinclair (1962). All material data given in Tables 1, 2 and S2 in supplementary material.

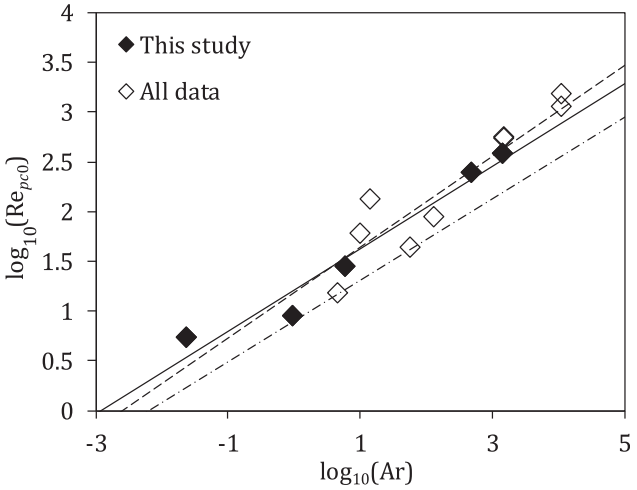

Fig. 6. Critical particle Reynolds number in dilute limit (or pick-up Reynolds number), Re_{pc0}, *vs.* Archimedes number, Ar. Closed diamonds: species used in this study (five); open diamonds: all datasets (14). Solid line: fit to present data. Dashed line: fit to all data. Dashed-dotted (lower) line: pick-up (Re_{pc0}) correlation of Soepyan et al. (2014).

Eq. (4), a material with a higher value of α will tend to have a higher critical deposition velocity at a given solids concentration, as α modifies the $\phi^{0.5}$ term. The results are shown in Fig. 8 and the relationship given in Eq. (9), where the goodness of fit was R^2 = 0.843: maximum packing fraction correlates well with volume factor. Conversely, Eq. (9) allows maximum packing fraction, an important parameter for rheological modelling, to be estimated from CDV data alone.

$$\alpha = 0.160\exp(6.68\phi_m). \tag{9}$$

Overall, the volume factor α might be viewed as a measure of the deviation from ideal hard-sphere behaviour, implicitly incorporating factors such as surface interactions and cohesion/aggregation, particle shape and roughness, for example, none of which are accounted for in the Archimedes number but which strongly influence packing fraction and the tendency to form a space-filling network. In order to quantify this deviation from ideal behaviour, it is noted that both Brouwers (2014) and Farr (2013) give expressions for the maximum packing fraction, ϕ_m, for non-interacting, hard-sphere particles with a log-normal size distribution. That given by Farr (2013) is used here as it is simpler to implement, taking only a measure of the width of the particle size distribution as an argument, and is as given in Eq. (10):

$$\phi_{\text{Farr}} = 1 - 0.57\exp(-S) + 0.2135\exp(-0.57S/0.2135) + 0.0019\left[\cos\left(2\pi\left[1 - \exp(-0.75S^{0.7} - 0.025S^4)\right]\right) - 1\right] \tag{10}$$

where S, along with M, are the logarithmic standard deviation and mean of a log-normal particle size distribution, respectively, such that the log-normal cumulative distribution function for a particle size d is as given in Eq. (11):

$$C(d) = \frac{1}{2}\left[1 + \text{erf}\left(\frac{\ln d - M}{S\sqrt{2}}\right)\right], \tag{11}$$

where erf is the error function. M and S for the particle species used here are given in Table 2 and were found *via* Eq. (11) using the sizing data (in μm units) given in Table 1.

The Farr (2013) model applies to ideal, non-interacting spheres and so represents a theoretical maximum in the packing fraction. Very high packing fractions are possible for species with wide size distributions, ultimately because smaller particles can fit into the interstices between larger ones. In the simple case of a bidisperse species – *i.e.*, two distinct sizes, and a large size ratio of the order of ten so that the particles of the smaller fraction fits fully between the larger (McGeary, 1961) – and assuming each size fraction reaches the random close packing (RCP) limit of ϕ_m = 0.64 (Gondret and Petit, 1997; Torquato et al., 2000), the "ultimate packing fraction" (Sudduth, 1993) in the bidisperse case is ϕ_m = 0.870. For a five-fraction species with similarly high size ratios, the figure is 99.4%. McGeary (1961) obtained real packings of up to 95.1% experimentally with metal spheres with quaternary size distributions; very high packings of spheres, cubes and cylinders were also modelled and compared with experimental data from the literature by Liu and Ha (2002). In numerical experiments, Desmond and Weeks (2014) found that both the skewness and relative width of spheres with linear, Gaussian and log-normal (*i.e.*, continuous) size distributions strongly influenced the packing density.

However, packings of real particles will exhibit some degree of deviation from this ideal behaviour and therefore a lower packing

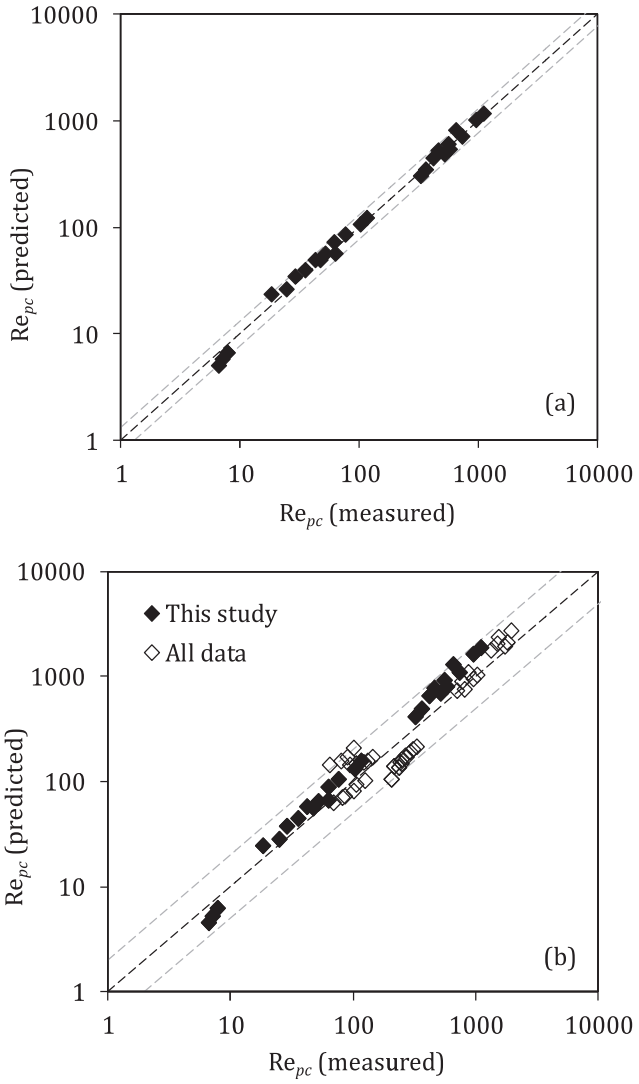

Fig. 7. Comparison of measured and predicted critical particle Reynolds number, Re_{pc}. (a) Data from present study and predicted values from Eq. (7), 26 data, grey dotted lines: ±30%; (b) all data and predicted values from Eq. (8), 64 data; grey dotted lines: ±100%.

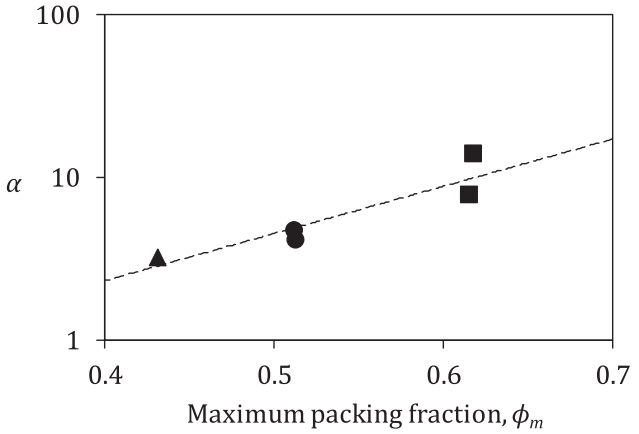

Fig. 8. Volume factor, α, *vs.* maximum packing fraction, ϕ_m, of solid phase for five particle species used in present study (two glass: squares, two plastic: circles, barytes: triangle) with exponential fit (dashed line). Values of α and ϕ_m given in Table 2.

fraction, whether as a result of (a) physical properties like roughness and non-sphericity, for example, or (b) surface forces and interparticle interactions that may cause aggregation and/or a more loosely packed settled bed. In fact, packing fractions as low as 1% have been found with nanoparticle species (Mizuno et al., 1991), in which interparticle forces are very high (Dong et al., 2006).

It is important also to highlight the influence of particle characteristics on measured maximum packing fractions. It is clear from Table 2 that the maximum packing fraction, ϕ_m, of the glass species is closest to the ideal hard-sphere value, ϕ_{Farr}, as would be expected as they are near-spherical and smooth (Rice et al., 2014) and therefore close to ideal. The plastic species are, however, rough and non-spherical as described in Section 3 and (Rice et al., 2017) and ϕ_m/ϕ_{Farr} is lower in those cases. The ratio ϕ_m/ϕ_{Farr} is lower still for barium sulphate: its broad size distribution (as characterised by a high value of S) would yield a high packing fraction if the particles were ideal hard spheres. However, it is known that the barytes has a surface charge (Balastre et al., 1999; Bux et al., 2017) which reduces the potential for particle rearrangement during gravitational consolidation in a settled bed, resulting in a lower packing fraction in practice (Balastre et al., 2002; Mizuno et al., 1991).

So, in suspensions of non-spherical, slightly aggregating or surface-charged minerals, the real packing fraction can differ vastly from the ideal hard-sphere packing fraction – calculated, for example, using the Farr (2013) model – because of the difficulty of surface-charged particle or aggregate network rearrangement during settling (Balastre et al., 2002; Balastre et al., 1999; Bergström, 1992; Bergström et al., 1992; Michaels and Bolger, 1962). A high value of the volume factor will tend to enhance the CDV for a given solids volume fraction, and ideal-sphere packing fraction estimations are not good for interacting or non-spherical particles. For highly aggregated, flocculated or surface-charged systems, the physical significance of α is to increase the *effective volume* of solids, which incorporates fluid entrained in the particle network structure (Michaels and Bolger, 1962). As such, the rightmost term in Eq. (4), $\alpha\phi^{0.5}$ can be rewritten in a more intuitive form as $\phi_{eff}^{0.5}$, where $\phi_{eff} = \alpha^2\phi$.

It is noted that, perhaps counterintuitively, pipe diameter does not appear to be as significant an influence as other factors on CDV. The dependence of CDV on conduit diameter found by other reviews, *e.g.*, Oroskar and Turian (1980) and Turian et al. (1987), is generally weak; Cabrejos and Klinzing (1994) for example, found a $U_c \propto D^{0.25}$ dependence. In addition, four datasets taken from Graf et al. (1970), as summarized in Tables S2 and S2 in the supplementary material, show only a small variation in Re_{pc} between experiments in pipes with two diameters. However, the difference in D is small (D = 101.6 and 152.4 mm). The range of pipe diameters in the datasets used here cover only about an order of magnitude; assuming a $D^{0.25}$ dependence, this corresponds to a ± 78% variation in U_c, *i.e.*, within the bounds (±100%) indicated in Fig. 7(b).

7. Conclusions

New experiments using five types of particles (two glass, two plastic and barytes) and solid concentrations up to 15% by volume have been undertaken, thereby extending a recent review (Soepyan et al., 2014) in the dilute limit and a previous study (Rice et al., 2015) at concentrations up to 5%. The results were integrated with data from the literature in order to establish a correlation between material and flow properties for prediction of the critical deposition velocity (CDV) in a range of multiphase flows consisting of both ideal and non-ideal solid particles, and a relationship between particle packing fraction and CDV is presented.

With respect to the issue of packing fraction and its influence on CDV, in general, any correlation that is able to predict CDV in a range of flows of industrial interest must be able to account, implicitly or explicitly, for the highly non-ideal behaviour of the majority of particle species for which data exist in the literature. Not only is this information (most importantly, particle size distribution, maximum packing fraction particle shape/roundness, tendency to aggregate, and more generally, surface properties such as the zeta potential, for example) often not reported by researchers, it is also difficult to account for theoretically in a model. The suggestion made here is that the maximum packing fraction and the discrepancy between it and the hard-sphere value for a given particle size distribution be used as a measure of, and proxy for, the deviation of a particle species from ideal behaviour. This discrepancy is quantified by the volume factor, which provides a valuable simplification. The empirical volume factor, α, was found to correlate well with measured maximum packing fraction. Although other proxies may be more suitable, none are forthcoming in the literature, and the discussion presented here of the influence of particle properties on the CDV is unlikely to be resolved without new high-quality experimental data that (a) incorporate full material characterisation, as outlined above and (b) cover the range of material properties likely to be encountered by operators in a range of industries in which hydraulic conveying of solids takes place. Consequently, the empirical volume factor provides an approach to extending the estimation of CDV to a much broader range of particles, and across a greater range of concentrations than has hitherto been demonstrated.

As to the future of research in this area, the method of zero bed-depth identification used here breaks down for sediments of interacting particles or any solids close to the gel point or other limiting packing fraction (and it is noted that there is a range of overlapping definitions), as the onset of hindered or very slow settling means a bed will not form within the measurement timescale, so the concept of bed depth becomes nebulous. More ambiguous but well established experimental methods, such as minimum pressure-drop identification, must then be used, in which case care must be taken when comparing results derived using different methods (Doron and Barnea, 1995; Thomas, 1961): Bain and Bonnington (1970) found that the critical velocity corresponding to minimum pressure drop generally exceeds the critical deposition velocity, and it may be possible to develop a consistent method to estimate one from the other.

Declaration of Competing Interest

The authors declared that there is no conflict of interest.

Acknowledgements

The authors thank Peter Dawson, Bob Harris, Tony Windross, Gareth Keevil and Robert Thomas for their technical assistance, and Olivier Mariette at Met-*Flow*, Switzerland, for his support and advice. The authors also thank the U.K. Engineering and Physical Sciences Research Council (EPSRC) for financial support of this study through grant EP/L014041/1: Decommissioning, Immobilisation and Storage Solutions for Nuclear Waste Inventories (DISTINCTIVE). We also warmly thank the editor and three anonymous reviewers for their comments, which improved the paper.

Appendix A. Supplementary material

Supplementary data to this article can be found online at https://doi.org/10.1016/j.ces.2019.115308.

References

Al-lababidi, S., Yan, W., Yeung, H., 2012. Sand transportations and deposition characteristics in multiphase flows in pipelines. J. Energ. Resour. Technol.-ASME 134, (13p.) 034501.

Babcock, H., Year, The sliding bed flow regime. In: "Hydrotransport 1", First International Conference on Hydraulic Transportation of Solids in Pipes, 1st-4th September 1970 University of Warwick, British Hydromechanics Research Association, H1-1-16.

Bain, A.G., Bonnington, S.T., 1970. The Hydraulic Transport of Solids by Pipeline. Pergamon Press, Oxford.

Balastre, M., Argillier, J.F., Allain, C., Foissy, A., 2002. Role of polyelectrolyte dispersant in the settling behaviour of barium sulphate suspension. Colloids Surf A 211, 145–156.

Balastre, M., Persello, J., Foissy, A., Argillier, J.F., 1999. Binding and ion-exchange analysis in the process of adsorption of anionic polyelectrolytes on barium sulfate. J. Colloid Interface Sci. 219, 155–162.

Bergström, L., 1992. Sedimentation of flocculated alumina suspensions: γ-ray measurements and comparison with model predictions. J. Chem. Soc Faraday Trans. 88, 3201–3211.

Bergström, L., Schilling, C.H., Aksay, I.A., 1992. Consolidation behavior of flocculated alumina suspensions. J. Am. Ceram. Soc. 75, 3305–3314.

Brouwers, H.J.H., 2014. Packing fraction of particles with lognormal size distribution. Phys. Rev. E 89, (12p.) 052211.

Bux, J., Paul, N., Hunter, T.N., Peakall, J., Dodds, J.M., Biggs, S., 2017. In situ characterization of mixing and sedimentation dynamics in an impinging jet ballast tank via acoustic backscatter. AIChE J. 63, 2618–2629.

Cabrejos, F.J., Klinzing, G.E., 1994. Pickup and saltation mechanisms of solid particles in horizontal pneumatic transport. Powder Technol. 79, 173–186.

Cairns, R., Lawther, K., Turner, K., 1960. Flow characteristics of dilute small particle suspensions. Brit. Chem. Eng. 5, 849–856.

Clark, A.H., Shattuck, M.D., Ouellette, N.T., O'Hern, C.S., 2015. Onset and cessation of motion in hydrodynamically sheared granular beds. Phys. Rev. E 92, (7p.) 042202.

Corey, A.T., 1949, Influence of shape on the fall velocity of sand grains, M.Sc., Colorado Agricultural and Mechanical College.

Crowe, C.T., 2006. Multiphase Flow Handbook. CRC Press, Taylor & Francis, Boca Raton.

Desmond, K.W., Weeks, E.R., 2014. Influence of particle size distribution on random close packing of spheres. Phys. Rev. E 90, (6p.) 022204.

Dietrich, W.E., 1982. Settling velocity of natural particles. Water Resour Res. 18, 1615–1626.

Dong, K.J., Yang, R.Y., Zou, R.P., Yu, A.B., 2006. Role of interparticle forces in the formation of random loose packing. Phys. Rev. Lett. 96, (4p.) 145505.

Doron, P., Barnea, D., 1995. Pressure drop and limit deposit velocity for solid-liquid flow in pipes. Chem. Eng. Sci. 50, 1595–1604.

Doron, P., Barnea, D., 1996. Flow pattern maps for solid-liquid flow in pipes. Int. J. Multiphas. Flow 22, 273–283.

Durand, R. and Condolios, E., 1952, The hydraulic transport of coal and solids materials in pipes. In: Colloquium on the Hydraulic Transport of Coal, 1952, London, National Coal Board.

Farr, R.S., 2013. Random close packing fractions of lognormal distributions of hard spheres. Powder Technol. 245, 28–34.

Gillies, R.G., Shook, C.A., 1991. A deposition velocity correlation for water slurries. Can. J. Chem. Eng. 69, 1225–1228.

Gillies, R.G., Shook, C.A., Wilson, K.C., 1991. An improved two layer model for horizontal slurry pipeline flow. Can. J. Chem. Eng. 69, 173–178.

Goedde, E., 1978, To the critical velocity of heterogeneous hydraulic transport. In: "Hydrotransport 5", Fifth International Conference on Hydraulic Transportation of Solids in Pipes, 8-11 May 1978 1978, Hannover, BHRA Fluid Engineering, Paper B4.

Gondret, P., Petit, L., 1997. Dynamic viscosity of macroscopic suspensions of bimodal sized solid spheres. J. Rheol. 41, 1261–1274.

Graf, W.H., Robinson, M.P., Yucel, O., 1970. Critical velocity for solid-liquid mixtures, Fritz Laboratory Reports, Paper 386. Lehigh University, Bethlehem, PA.

Hayden, J.W., Stelson, T., Zandi, I., 1971. Hydraulic conveyance of solids in pipes. In: Zandi, I. (Ed.), Advances in Solid-Liquid Flow in Pipes and Its Applications. Pergamon Press, Oxford.

Hughmark, G., 1961. Aqueous transport of settling slurries. Ind. Eng. Chem. 53, 389–390.

Hunter, T.N., Peakall, J., Unsworth, T.J., Acun, M.H., Keevil, G., Rice, H., Biggs, S., 2013. The influence of system scale on impinging jet sediment erosion: Observed using novel and standard measurement techniques. Chem. Eng. Res. Des. 91, 722–734.

Johnson, M., Peakall, J., Fairweather, M., Biggs, S., Harbottle, D., Hunter, T.N., 2016. Characterization of multiple hindered settling regimes in aggregated mineral suspensions. Ind. Eng. Chem. Res. 55, 9983–9993.

Liddell, K.C., Burnett, D.F., 2000. Critical Transport Velocity: A Review of Correlations and Models, RPP-7185 (Rev. 0). Hanford Group, Inc., Richland, Washington.

Liu, S.J., Ha, Z.Y., 2002. Prediction of random packing limit for multimodal particle mixtures. Powder Technol. 126, 283–296.

McGeary, R.K., 1961. Mechanical packing of spherical particles. J. Am. Ceram. Soc. 44, 513–522.

Michaels, A.S., Bolger, J.C., 1962. Settling rates and sediment volumes of flocculated kaolin suspensions. Ind. Eng. Chem. Fundam. 1, 24–33.
Miedema, S.A., 2016. The heterogeneous to homogeneous transition for slurry flow in pipes. Ocean Eng. 123, 422–431.
Mizuno, M., Fukaya, A., Jimbo, G., 1991. The estimation of packing characteristics by centrifugal compaction of ultrafine particles. KONA Powder Part J. 9, 19–27.
Murphy, G., Young, D.F. and Burian, R.J., 1954, Progress report on friction loss of slurries in straight tubes, ICS-474: U.S. Atomic Energy Commission.
Newitt, D., 1955. Hydraulic conveying of solids in horizontal pipes. Trans. Inst. Chem. Eng. 33, 93–113.
Oroskar, A.R., Turian, R.M., 1980. The critical velocity in pipeline flows of slurries. AlChE J. 26, 550–558.
Parzonka, W., Kenchington, J.M., Charles, M.E., 1981. Hydrotransport of solids in horizontal pipes: effects of solid concentration and particle size on the deposit velocity. Can. J. Chem. Eng. 59, 291–296.
Paul, N., Biggs, S., Edmondson, M., Hunter, T.N., Hammond, R.B., 2013. Characterising highly active nuclear waste simulants. Chem. Eng. Res. Des. 91, 742–751.
Paul, N., Biggs, S., Shiels, J., Hammond, R.B., Edmondson, M., Maxwell, L., Harbottle, D., Hunter, T.N., 2017. Influence of shape and surface charge on the sedimentation of spheroidal, cubic and rectangular cuboid particles. Powder Technol. 322, 75–83.
Peker, S.M., Helvacı, S.S., 2007. Solid-Liquid Two Phase Flow. Elsevier, Amsterdam.
Peysson, Y., Ouriemi, M., Medale, M., Aussillous, P., Guazzelli, E., 2009. Threshold for sediment erosion in pipe flow. Int. J. Multiphas. Flow 35, 597–600.
Poloski, A.P., Etchells, A.W., Chun, J., Adkins, H.E., Casella, A.M., Minette, M.J., Yokuda, S.T., 2010. A pipeline transport correlation for slurries with small but dense particles. Can. J. Chem. Eng. 88, 182–189.
Powers, M.C., 1953. A new roundness scale for sedimentary particles. J. Sediment. Res. 23, 117–119.
Rabinovich, E., Kalman, H., 2011. Threshold velocities of particle-fluid flows in horizontal pipes and ducts: literature review. Rev. Chem. Eng. 27, 215–239.
Rice, H.P., 2013. Transport and deposition behaviour of model slurries in closed pipe flow. University of Leeds, Ph.D.
Rice, H.P., Fairweather, M., Hunter, T.N., Mahmoud, B., Biggs, S., Peakall, J., 2014. Measuring particle concentration in multiphase pipe flow using acoustic backscatter: Generalization of the dual-frequency inversion method. J. Acoust. Soc. Am. 136, 156–169.
Rice, H.P., Fairweather, M., Hunter, T.N., Peakall, J., Biggs, S.R., 2017. The influence of relative fluid depth on initial bedform dynamics in closed, horizontal pipe flow. Int. J. Multiphas. Flow 93, 1–16.
Rice, H.P., Fairweather, M., Peakall, J., Hunter, T.N., Mahmoud, B., Biggs, S.R., 2015. Constraints on the functional form of the critical deposition velocity in solid-liquid pipe flow at low solid volume fractions. Chem. Eng. Sci. 126, 759–770.
Richardson, J.F., Zaki, W.N., 1954. The sedimentation of a suspension of uniform spheres under conditions of viscous flow. Chem. Eng. Sci. 3, 65–73.
Sinclair, C.G., 1962, The limit deposit-velocity of heterogeneous suspensions. In: Symposium on the Interaction between Fluids and Particles: Third Congress of the European Federation of Chemical Engineers, 1962, London, Institution of Chemical Engineers, 79p.
Smith, R., 1955. Experiments on the flow of sand water slurries in horizontal pipes. Trans. Inst. Chem. Eng. 33, 85–92.
Soepyan, F.B., Cremaschi, S., Sarica, C., Subramani, H.J., Kouba, G.E., 2014. Solids transport models comparison and fine-tuning for horizontal, low concentration flow in single-phase carrier fluid. AlChE J. 60, 76–112.
Spells, K.E., 1955. Correlations for use in transport of aqueous suspension of fine solids through pipes. Trans. Inst. Chem. Eng., 79–84
Sudduth, R.D., 1993. A new method to predict the maximum packing fraction and the viscosity of solutions with a size distribution of suspended particles. II. J. Appl. Polym. Sci. 48, 37–55.
Syvitski, J.P.M. (Ed.), 2007. Principles, Methods and Application of Particle Size Analysis. Cambridge University Press, Cambridge.
Thomas, A.D., 1979. Predicting the deposit velocity for horizontal turbulent pipe flow of slurries. Int. J. Multiphas. Flow 5, 113–129.
Thomas, D.G., 1961. Transport characteristics of suspensions: Part II Minimum transport velocity for flocculated suspensions in horizontal pipes. AlChE J. 7, 423–430.
Thomas, D.G., 1962. Transport characteristics of suspensions: Part VI minimum transport velocity for large particle size suspensions in round horizontal pipes. AlChE J. 8, 373–378.
Torquato, S., Truskett, T.M., Debenedetti, P.G., 2000. Is random close packing of spheres well defined? Phys. Rev. Lett. 84, 2064–2067.
Turian, R.M., Hsu, F.L., Ma, T.W., 1987. Estimation of the critical velocity in pipeline flow in slurries. Powder Technol. 51, 35–47.
Vesilind, P.A., 1968. Design of prototype thickeners from batch settling tests. Water Sewage Works 115, 302–307.
Wasp, E.J., Kenny, J.P., Gandhi, R.L., 1977. Solid-Liquid Flow Slurry Pipeline Transportation. Trans-Tech Publications, Clausthal.
Welch, T.D., 2001. Tank Waste Transport, Pipeline Plugging, and the Prospects for Reducing the Risk of Waste Transfers. Oak Ridge National Laboratory, Oak Ridge.
Wilson, K.C., 1965, Derivation of the regime equations from relationships for pressurized flow by use of the principle of minimum energy - degradation rate, Civil Engineering Research Report No. 51, Kingston, Ontario: Queen's University.
Worster, R., Denny, D., 1955. Hydraulic transport of solid material in pipes. Proc. Inst. Mech. Eng. 169, 563–586.